



Early amyloid-induced changes in microglia gene expression in male APP/PS1 mice

Takuya Oshima¹  | Mandy S. J. Kater²  | Christiaan F. M. Huffels³  | Evelyn M. Wesseling¹ | Jinte Middeldorp^{3,4} | Elly M. Hol³ | Mark H. G. Verheijen²  | August B. Smit² | Erik W. G. M. Boddeke^{1,5} | Bart J. L. Eggen¹ 

¹Department of Biomedical Sciences, Section Molecular Neurobiology, University Medical Center Groningen, University of Groningen, Groningen, The Netherlands

²Department of Molecular and Cellular Neurobiology, Center for Neurogenetics and Cognitive Research, Amsterdam Neuroscience, Vrije Universiteit Amsterdam, Amsterdam, The Netherlands

³Department of Translational Neuroscience, University Medical Center Utrecht Brain Center, Utrecht University, Utrecht, The Netherlands

⁴Department of Neurobiology & Aging, Biomedical Primate Research Centre, Rijswijk, The Netherlands

⁵Department of Cellular and Molecular Medicine, Center for Healthy Aging, University of Copenhagen, Copenhagen, Denmark

Correspondence

Bart J. L. Eggen, Department of Biomedical Sciences, Section Molecular Neurobiology, University Medical Center Groningen, University of Groningen, Antonius Deusinglaan 1, 9713 AV Groningen, The Netherlands.
Email: bj.l.eggen@umcg.nl

Funding information

ZonMw, Grant/Award Number: 733050816

Abstract

Alzheimer's disease (AD) is a progressive neurodegenerative disease and the most common cause of dementia, characterized by deposition of extracellular amyloid-beta (A β) aggregates and intraneuronal hyperphosphorylated Tau. Many AD risk genes, identified in genome-wide association studies (GWAS), are expressed in microglia, the innate immune cells of the central nervous system. Specific subtypes of microglia emerged in relation to AD pathology, such as disease-associated microglia (DAMs), which increased in number with age in amyloid mouse models and in human AD cases. However, the initial transcriptional changes in these microglia in response to amyloid are still unknown. Here, to determine early changes in microglia gene expression, hippocampal microglia from male APP^{swe}/PS1^{dE9} (APP/PS1) mice and wild-type littermates were isolated and analyzed by RNA sequencing (RNA-seq). By bulk RNA-seq, transcriptomic changes were detected in hippocampal microglia from 6-months-old APP/PS1 mice. By performing single-cell RNA-seq of CD11c-positive and negative microglia from 6-months-old APP/PS1 mice and analysis of the transcriptional trajectory from homeostatic to CD11c-positive microglia, we identified a set of genes that potentially reflect the initial response of microglia to A β .

KEYWORDS

Alzheimer's disease, amyloid, microglia, neuroinflammation, RNA-seq, RRID:AB_313038, RRID:AB_313776, RRID:AB_465051, RRID:AB_467134, RRID:AB_839504, RRID:AB_2056966, RRID:AB_2336180, RRID:AB_2340593, RRID:AB_2563061, RRID:AB_2629529, RRID:AB_11203704

1 | INTRODUCTION

Alzheimer's disease (AD) is a progressive neurodegenerative disease characterized by memory impairment and cognitive decline.

About one in nine people above 65 is diagnosed with AD in the US, and the number of AD patients in western societies is increasing rapidly (Alzheimer's Association, 2022). AD features several pathological hallmarks, such as brain atrophy, abnormal

Mandy S. J. Kater and Christiaan F. M. Huffels contributed equally to this work.

Edited by Junie Paula Warrington and Luana Fioriti. Reviewed by Aniko Korosi.

This is an open access article under the terms of the [Creative Commons Attribution](https://creativecommons.org/licenses/by/4.0/) License, which permits use, distribution and reproduction in any medium, provided the original work is properly cited.

© 2024 The Authors. *Journal of Neuroscience Research* published by Wiley Periodicals LLC.

extracellular aggregates of amyloid-beta ($A\beta$), intraneuronal neurofibrillary tangles formed by the accumulation of hyperphosphorylated tau protein, and loss of neurons and synapses (DeTure & Dickson, 2019). AD is categorized into two types: familial AD and sporadic AD. Most of the familial AD cases are early in onset and are caused by autosomal dominant inheritance of mutations in genes such as Amyloid Precursor Protein (APP) (Goate et al., 1991), Presenilin-1 (PSEN1) (Campion et al., 1995), and Presenilin-2 (PSEN2) (Sherrington et al., 1996). On the other hand, sporadic AD, which accounts for more than 95% of all AD cases, typically has an onset after the age of 65 years. Although the etiology of sporadic AD has not been determined yet, genome-wide association studies (GWAS) identified late-onset AD risk genes, of which many have been associated with microglia, the innate immune cells of the central nervous system (CNS) (Jansen et al., 2019; Wightman et al., 2021). In addition, several signs of neuroinflammation such as upregulation of inflammatory cytokines and chemokines have been observed in AD patients (Cribbs et al., 2012; Morimoto et al., 2011; Tarkowski et al., 2003), indicating a key role for microglia in the etiology of AD.

Microglia around $A\beta$ plaques exhibit a distinct morphology and gene expression profile compared to microglia in seemingly less affected parenchyma in AD amyloid mouse models (Chen et al., 2020; Kamphuis et al., 2016; Plescher et al., 2018; Yin et al., 2017). Previous studies with amyloid mouse models identified subsets of amyloid-associated microglia including "disease-associated microglia (DAMs)", which highly express genes related to inflammatory responses and phagocytosis (Chen et al., 2020; Hemonnot-Girard et al., 2022; Keren-Shaul et al., 2017; Krasemann et al., 2017; Sala Frigerio et al., 2019). Recently, DAMs have been classified into two ontogenetically and functionally distinct cell lineages: embryo-derived neuroprotective DAMs and monocyte-derived disease inflammatory macrophages (DIMs) (Silvin et al., 2022). An amyloid-associated subtype of microglia was also detected in post-mortem brain tissue of AD patients with gene expression profiles similar to DAMs (Gerrits et al., 2021). However, how microglia are triggered by $A\beta$ and subsequently acquire this gene expression signature at the early stages of AD is still unknown.

APP^{swe}/PSEN1^{dE9} (APP/PS1) is an amyloid mouse model, which develops prominent $A\beta$ deposits in the hippocampus by the age of 4–6 months (Jankowsky et al., 2004; Kater et al., 2023), which is a relatively late compared to other, more aggressive, amyloid mouse models such as 5xFAD. Interestingly, APP/PS1 mice exhibit cognitive impairment and microgliosis at the age of 3 months, even before $A\beta$ deposits are detected (Kater et al., 2023; Vegh et al., 2014). Here, we used APP/PS1 mice to determine early transcriptional changes in microglia in response to $A\beta$. We performed RNA sequencing of hippocampal microglia and investigated the transcriptional trajectory from homeostatic microglia to DAMs in order to identify the early changes in microglia gene expression in APP/PS1 mice.

Significance

This study reveals new insights into the early transcriptional changes of microglia in response to amyloid-beta ($A\beta$) in Alzheimer's disease (AD). Using bulk and single-cell RNA sequencing, we identified a set of genes that potentially reflect the initial response of microglia to $A\beta$, which is distinct from the previously reported disease-associated microglia (DAM) genes. These findings shed light on the role of microglia in the initial stages of AD amyloid pathology.

2 | METHODS

2.1 | Animals

APP/PS1 mice (Jackson Laboratory strain B6C3-Tg (APP^{swe},PSEN1^{dE9})85Dbo/J; stock number 004462) express a chimeric mouse/human amyloid precursor protein (APP) gene with the Swedish double mutation K595N/M596L (APP^{swe}) and a human PS1 gene in which exon 9 is deleted (PS1^{dE9}), under the control of the mouse prion protein promoter (MoPrP.Xho) (Jankowsky et al., 2004). Hemizygous male and female APP/PS1 and wild-type (WT) littermates were bred in-house and maintained on a C57BL/6 background. Males and females were separated at weaning and were housed in different cages. Mice were group housed in cages with sawdust bedding, nesting material, a PVC-tube and a gnawing stick. Number of animals was dependent on the litter with a maximum of four animals per cage. Housing was controlled for temperature (~21°C), humidity (~50%–55%), and 12 h light-dark cycle. The cages were cleaned once a week. The animals were not handled for the experiments in this study except for a single injection for anesthesia followed by perfusion. All experimental procedures were approved by the Central Committee on Animal Experiments in the Netherlands (CCD) and the animal ethical care committee (DEC) of the Vrije Universiteit Amsterdam (approval protocol AVD1120020174287) and Utrecht University (AVD1150020174314) and complied with the European Council Directive (2010/63/EU).

2.2 | Immunohistochemistry

Male APP/PS1 and WT mice at the age of 4 and 6 months ($n = 3$ animals per group) were used for immunohistochemistry. After mice were sacrificed by perfusion with ice-cold phosphate-buffered saline (PBS) under anesthesia with 3.5% isoflurane, the whole brains were removed from the skull and kept in cold PBS. The brains were fixed in 4% paraformaldehyde (PFA) in PBS at 4°C for 24 h, followed by cryo-preservation in 30% sucrose in PBS at 4°C for 48 h. The brain was cut in sagittal sections of 16 μ m thickness using a cryostat microtome and mounted on microscope slides. The

brain sections on the slides were placed in 10 mM sodium citrate (pH = 6.0), and heat-induced epitope retrieval was performed in a microwave for 10 min. Then, blocking of endogenous peroxidase activity was performed using .3% hydrogen peroxide in PBS at room temperature for 30 min. After blocking in 5% normal donkey serum in PBS with .1% Triton X-100 (Sigma, cat#93443) at room temperature for 1 h, the samples were incubated in PBS containing anti-IBA1 (WAKO, cat#019-19741, [RRID:AB_839504](#), 1:1000) or anti-A β (DAKO, cat#M0872, [RRID:AB_2056966](#), 1:100) with .1% Triton X-100 and 1% normal donkey serum at 4°C overnight. After incubation with biotinylated secondary anti-rabbit IgG antibody (Jackson ImmunoResearch, cat#711-065-152, [RRID:AB_2340593](#), 1:400) for IBA1 or anti-mouse IgG antibody (Vector, cat#BA-2001, [RRID:AB_2336180](#), 1:400) for A β at room temperature for 1 h, the samples were incubated with ABC solution (VECTASTAIN® ABC Kit, Vector Laboratories, cat#PK-6100) at room temperature for 30 min. Finally, IBA1- and A β - immunoreactivity was visualized using 3,3'-diaminobenzidine (DAB). The whole brain sections were scanned on a NanoZoomer 2.0-HT scanner (Hamamatsu Photonics) at 40 \times magnification.

2.3 | Microglia and A β plaque density analysis

Microglia and A β plaque density in cornu ammonis (CA) and dentate gyrus (DG) were determined by using the cell counter plugin for ImageJ software (<http://rsb.info.nih.gov/ij/>) to count Iba1-positive cells and A β plaques manually and calculate region areas (mm²) on 8 \times magnification images. The experimenter was blinded for the experimental conditions when counting microglia. Three mice per group (one brain section per mouse) were used.

2.4 | Microglia morphometric analysis

Single-cell images of microglia were selected and processed for morphometric analysis as described previously (van Weering et al., 2023; Zhang et al., 2021). A list of the morphometric parameters with explanations is provided in Supplemental Table S1. A hierarchical clustering on principal components approach was used to identify and compare microglia subpopulations between experimental groups.

2.5 | Bulk RNA sequencing

2.5.1 | Tissue dissociation and microglia isolation by fluorescence-activated cell sorting (FACS)

Male APP/PS1 and WT mice at the age of 4, 6, and 9 months ($n = 10$ per group) were used for microglia isolations and sequencing. Microglia were isolated using an enzymatic protocol at 4°C as previously described (Talma et al., 2021). Briefly, after the whole

PBS-perfused brains were removed, the hippocampi were carefully removed, followed by GentleMACS dissociation in a mixture of 15 mg/mL Protease (Sigma, cat#P5380), 1 mL-cysteine hydrochloride (Sigma, cat#C7477) and .5 μ g/ μ L DNase (Roche, cat#10104159001) at 4°C. After centrifugation (300 rcf, 4°C, 10 min) of the homogenates that were passed through a 100 μ m cell strainer (Corning, cat#352360), myelin removal was performed by resuspending the pellets in 25 mL 24% percoll (Fisher, cat#17-0891-01) in medium A (HBSS (Gibco, cat#14170-088) with .6% glucose (Sigma, cat#G8769) and 7.5 mM HEPES (pH = 7.2–7.5) (Lonza, cat#BE17-737E)) with 3 mL PBS layered on top, followed by centrifugation (950 rcf, 4°C, 20 min, decreased acceleration and no brake). The cell pellets were resuspended in 100 μ L of medium A without phenol red. To avoid unspecific binding of antibodies to cells, blocking of Fc receptors was performed with 1 μ L of CD16/CD32 antibody (eBioscience, cat#14-0161-85, [RRID:AB_467134](#), 1:100) for 5 min, and the cell pellets were stained with 1 μ L of CD11b-BV421 (Biolegend, cat#101236, [RRID:AB_11203704](#), 1:100), CD45-BV510 (Biolegend, cat#103138, [RRID:AB_2563061](#), 1:100) and CD49d-PE (Biolegend, cat#103607, [RRID:AB_313038](#), 1:100) antibodies on ice for 30 min. The cells were washed once and filtered into FACS tubes (Falcon, cat#352235). After adding 1 μ L of Propidium Iodide (PI, 1 mg/mL, Promokine, cat#pk-ca707-40,017) and DRAQ5 (5 mM, Thermo fisher, cat#62251) to the samples, microglia were sorted by gating the PI^{neg} DRAQ5^{pos} CD11b^{high} CD45^{int} CD49d^{neg} cells using the Beckman Coulter MoFlo Astrios or XDP (Figure S2). Microglia were collected in siliconized tubes (Sigma, cat#T3406-250EA) containing RLT+ buffer in RNeasy Micro Kit (Qiagen, cat#74004) and stored at -80°C. Flow cytometry data were analyzed using Kaluza Analysis Software (Beckman Coulter).

2.5.2 | RNA isolation and RNA sequencing

Total RNA was isolated using RNeasy Micro Kit (Qiagen, cat#74004) according to the manufacturer's instructions. Microglia from two or three mice with the same condition were pooled in this step to obtain a minimum of 1.5 ng RNA for RNA-sequencing ($n = 4$ per group after pooling). RNA concentrations were measured using Fragment Analyzer RNA Kits (Agilent, cat#DNF-472). Sequencing libraries were generated using the NEBNext Low Input RNA Library Prep Kit for Illumina (New England Biolabs, cat#E6420S/L) by Genomescan. Briefly, cDNA which was synthesized and amplified from poly A tailed mRNA which was used for ligation with the sequencing adapters and PCR amplification of the resulting product. The quality and yield after sample preparation was measured with the Fragment Analyzer HS NGS Fragment Kits (Agilent, cat#DNF-474). The size of the resulting products was consistent with the expected size distribution (a peak between 200 and 400 bp). Clustering and DNA sequencing was performed using a NovaSeq6000 according to the manufacturer's protocols. NovaSeq control software NCS v1.7 was used. Image analysis, base calling, and quality check was performed with the Illumina data analysis pipeline RTA3.4.4 and Bcl2fastq v2.20.

2.5.3 | RNA sequencing analysis

FastQC (v0.11.9) and FastQA (v3.1.25) tools were used for quality control of the sequencing data, and cutadapt (v2.10) was used for adapter trimming. The trimmed reads were mapped to the mouse GRCm39 reference sequence (*Mus_musculus.GRCm39.dna.primary_assembly.fa*) by using Tophat (v2-2.1). After alignment, duplicate reads were removed with MarkDuplicates of the Picard package (v2.13.2), then transcripts were counted with HTSeq (v0.11.0). Downstream analysis was performed using R/Bioconductor packages (v.4.1.1) as previously demonstrated (Law et al., 2018). Three samples were detected as outliers during processing of the data (<10,000 total reads or because of a distinct transcriptomic profile due to technical reasons or contamination) and removed for further analyses. Genes with low expression (total counts <5) were filtered. The edgeR package (v3.36.0) (Robinson et al., 2010) and the limma package (v3.50.3) (Ritchie et al., 2015) were used for normalization, transformation, and differential gene expression analysis. A principal components analysis (PCA) was performed with the transposed form of log counts per million (logCPM) matrix and visualized in a PCA plot. Differentially expressed genes were detected with a threshold of adjusted *p*-value <.05.

2.6 | Single-cell RNA sequencing

2.6.1 | Tissue dissociation and microglia isolation by fluorescence-activated cell sorting (FACS)

Male APP/PS1 and WT mice at the age of 6 months ($n=4$ per group) were used for microglia isolation. Microglia were isolated using a mechanical protocol at 4°C as previously described (Galatro et al., 2017). Briefly, after the whole PBS-perfused brains were removed, the isocortex and hippocampi were carefully removed, followed by mechanical dissociation using a Tissue Grinder Potter-Elvehjem. After centrifugation of the homogenates that were passed through a 70 µm cell strainer (Corning, cat#352350), myelin was removed by resuspending the pellet in 25 mL 24% percoll (Fisher, cat#17-0891-01) in medium A (HBSS (Gibco, cat#14170-088) with .6% glucose (Sigma, cat#G8769) and 7.5 mM HEPES (Lonza, cat#BE17-737E)) with 3 mL PBS layered on top, followed by centrifugation. The cell pellets were resuspended in 100 µL of medium A without phenol red. Then, blocking was performed with 1 µL of CD16/CD32 antibody (eBioscience, cat#14-0161-85, RRID:AB_467134, 1:100) for 5 min, and the cell pellets were stained with 1 µL of CD11b-BV510 (Biolegend, cat#101263, RRID:AB_2629529, 1:100), CD45-FITC (eBioscience, cat#11-0451-85, RRID:AB_465051, 1:100), and CD11c-PE (Biolegend, cat#117307, RRID:AB_313776, 1:100) antibodies for 30 min on ice. The stained cells were washed once and filtered into FACS tubes. After adding 1 µL of DAPI (4',6-Diamidino-2-Phenylindole, 200 µg/mL, Dilactate, cat#42280) and DRAQ5 (5 mM, Thermo fisher, cat#62251) to the

samples, microglia were sorted by gating the DAPI^{neg} DRAQ5^{pos} CD11b^{high} CD45^{int} CD11c^{neg/pos} cells using the Beckman Coulter MoFlo Astrios or XDP (Figure S3). Microglia were collected in 384-well PCR plates containing cell lysis buffer (.2% Triton (Sigma-Aldrich, cat#T9284), 4 U RNase inhibitor (Takara, cat#2313A), 10 mM dNTPs (Thermo Fisher Scientific, cat#R0193), and 10 µM barcoded oligo-dT primer) and were stored at -80°C. Analysis of flow cytometry data including the determination of proportions of CD11c^{neg} and CD11c^{pos} microglia was performed by using Kaluza Analysis Software (Beckman Coulter).

2.6.2 | Library preparation

Library preparation was performed based on the Smart-seq2 protocol as previously described (Alsema et al., 2020). Briefly, after cell lysis and annealing with barcoded poly-dT primer, RNA was reverse transcribed (RT) with .1 µM biotinylated barcoded template switching oligo (BC-TSO, 5'-AAGCAGTGGTATCAACG CAGAGTACATrGrG+G-biotin-3'), 25 U SmartScribe reverse transcriptase, 1x first-strand buffer, and 2 mM DTT (Takara, cat#639538), 1 U RNase inhibitor (Takara, cat#2313A), and 1 M betaine (Sigma-Aldrich, cat#B0300-5VL). The barcoded poly-dT primer contains a cell-specific barcode and a unique molecular identifier (UMI) for performing multiplexing of cells and handling PCR amplification bias. After the RT reaction, primer-dimers and small fragments were removed by .5 U Exonuclease (GE Healthcare, cat#E70073Z) reaction. cDNA libraries were amplified with KAPA Hifi HotStart ReadyMix (KAPA Biosystems, cat#KK2602) and custom PCR primer (5'-AAGCAGTGGTATCA ACGCAGAGT-3'). After the amplification step, cDNA libraries of 84 cells were pooled and washed with AMPure XP beads (Beckman Coulter, cat#A63880). The quality and concentration of the cDNA libraries were measured with the Agilent High Sensitivity DNA Kit (Agilent, cat#5067-4626) on 2100 Bioanalyzer (Agilent). 500 pg of the cDNA libraries were tagmented and indexed with the Illumina Nextera XT DNA preparation kit (Illumina, cat#FC-131-1024) according to the manufacturer's protocol. The indexing PCR was performed with the pool-specific Nextera indices (Illumina, cat#FC-131-2001) and 10 µM P5-TSO hybrid primer (5'-AATGA TACGGCGACCACCGAGATCTACACGCCGTCCGCGGAAGCAG TGGTATCAACGCAGAGTAC-3'). After purification of the indexed cDNA libraries by AMPure XP beads, the quality and concentration of the cDNA libraries were measured again with Agilent High Sensitivity DNA Kit on 2100 Bioanalyzer. All the cDNA libraries were pooled in one superpool, and removal of primer dimers and purification of the superpool were performed by gel electrophoresis with 2% agarose gel (Invitrogen, cat#10135444) followed by DNA extraction with the ZymoClean Gel DNA Recovery kit (Zymo Research, cat#D4007). The quality and concentration of the superpool were measured with Agilent High Sensitivity DNA Kit on 2100 Bioanalyzer performing multiplexing of cells, and the superpool and .3 µM BC read 1 primer (5'-GCCTGTCCGCGGAAGCA

GTGGTATCAACGCAGAGTAC-3') were loaded and sequenced on Illumina NextSeq 500 system at a final concentration of 2 pM with a 7% spike in PhiX DNA.

2.6.3 | Preprocessing of RNA sequencing data

Reads from Smart-seq2 single-cell RNA-sequencing were pre-processed with a custom pipeline as described previously (Alsema et al., 2020). Briefly, raw reads were demultiplexed with UMI-tools (v0.5.3) (Smith et al., 2017). A cell barcode whitelist with the known barcodes was used to filter the reads. Reads were aligned with HISAT2 (v2.1.0) to the Ensembl genome *Mus musculus* (GRCm38, mm10) using default parameters. Quantification was done with featureCounts (v1.6.0) using the flag -primary. The unique molecules per gene and per cell were quantified using the UMI-tools function count (Smith et al., 2017).

2.6.4 | Downstream analysis

Downstream analysis was performed using R/Bioconductor packages (v.4.1.1) with the Seurat package (v.4.1.0) (Hao et al., 2021). Cells with less than 200 or more than 2500 unique genes and cells with >5% mitochondrial transcripts were excluded. Raw counts were normalized by total expression per cell, scaled by 10,000 and log-transformed. Clustering of the cells was performed with the first 10 principal components with cluster resolution at .6. Cluster-enriched genes were identified using logistic regression as implemented in FindAllMarkers function. Differentially expressed genes between clusters were detected with thresholds of $|\log_2\text{FoldChange}| > .25$ and adjusted p -value $< .05$ with FindAllMarkers function. Gene Ontology (GO) analysis was performed using ClusterProfiler package (v4.4.1) (Wu et al., 2021). GO terms in biological process were identified with their significant enrichment (adjusted p -value $< .05$). SynGO was used for synaptic GO analysis (Koopmans et al., 2019).

2.7 | Statistical analysis

Statistical analyses were performed by GraphPad Prism 8 (GraphPad Software Inc.). Normal distribution of the data was tested by quantile-quantile (QQ) plots. An unpaired Student's t -test was used for the comparison of the mean differences of two groups. Two-way analysis of variance (ANOVA) followed by Tukey's multiple comparisons test was used for the comparison of the mean differences of multiple groups. All the statistical information is summarized in Table S2. We conducted our experiments with a minimal sample size of $n=3$, anticipating low variance between animals. Three to four biological replicates (mice) for RNA-seq studies is a commonly used number. Furthermore, we aimed to minimize the use of animals by reducing the total number employed in the study.

3 | RESULTS

3.1 | Microglia density is increased in hippocampus of APP/PS1 mice prior to A β plaques accumulation

To determine A β accumulation in our APP/PS1 mice, we performed A β immunostaining on hippocampal sections of 4- and 6-month-old APP/PS1 and WT mice (Figure 1a). While almost no A β plaques were observed in 4-month-old APP/PS1 mice, on average, five A β plaques per mm² were observed in 6-month-old APP/PS1 mice in both the CA and DG of the hippocampus (Figure 1b,c). We also examined the size of A β plaques (Figure S1a). Six-month-old APP/PS1 mice exhibited various size of A β plaques, and many of the plaques were small (less than 400 μ m²). This data indicate that 6-month-old APP/PS1 mice can exhibit different states of microglia including the ones reacting to small amyloid particles or large A β plaques.

To investigate the density of microglia in the hippocampus, we stained the brain sections for IBA1. Microglia density was significantly increased in the CA of 4- and 6-month-old APP/PS1 mice but not in the DG (Figure 1d,e). Altogether, these results indicate that microglia density especially in the CA of the hippocampus already changes before the accumulation of A β in frequently detectable plaques occurs, in line with our previous observations (Kater et al., 2023).

To examine detailed morphological changes in microglia, we performed a morphometric analysis of microglia in CA in 4- and 6-month-old APP/PS1 mice by measuring 23 morphological parameters (Figure S1b, Table S1). Among the six different subtypes determined by hierarchical clustering (Figure S1c), cluster 6 microglia were smaller in size without ramified branches (Figure S1d-f). Cluster 6 microglia were exclusively detected in 6-month-old APP/PS1 mice (Figure S1g). Given that accumulation of microglia was observed in 6-month-old APP/PS1 mice (Figure 1d) and microglia accumulates around A β plaques (Yin et al., 2017), these cluster 6 microglia seem to be plaque-associated microglia. We did not detect major changes in morphology between WT and APP/PS1 mice at 4 months (Figure S1g), although we observed changes in microglia density. Altogether, these data indicate that only microglia around A β plaques change their morphology drastically.

3.2 | Transcriptomic changes in microglia were first detected in 6-month-old APP/PS1 mice

To investigate transcriptomic changes associated with the increase in microglia density in APP/PS1 mice, we isolated microglia from the hippocampus of 4-, 6-, and 9-month-old APP/PS1 and WT mice based on CD11b and CD45 expression by Fluorescence-Activated Cell Sorting (FACS), and performed RNA sequencing (RNA-seq) (Figures 2a and S3). Principal component analysis (PCA) was used to assess differences in gene expression profiles between samples (Figure 2b). Gene expression analysis (Log fold change (LFC) > 0 , adjusted p -value $< .05$) between 4-months-old APP/PS1 and WT mice revealed no differentially expressed genes (DEGs) (Figure 2c).

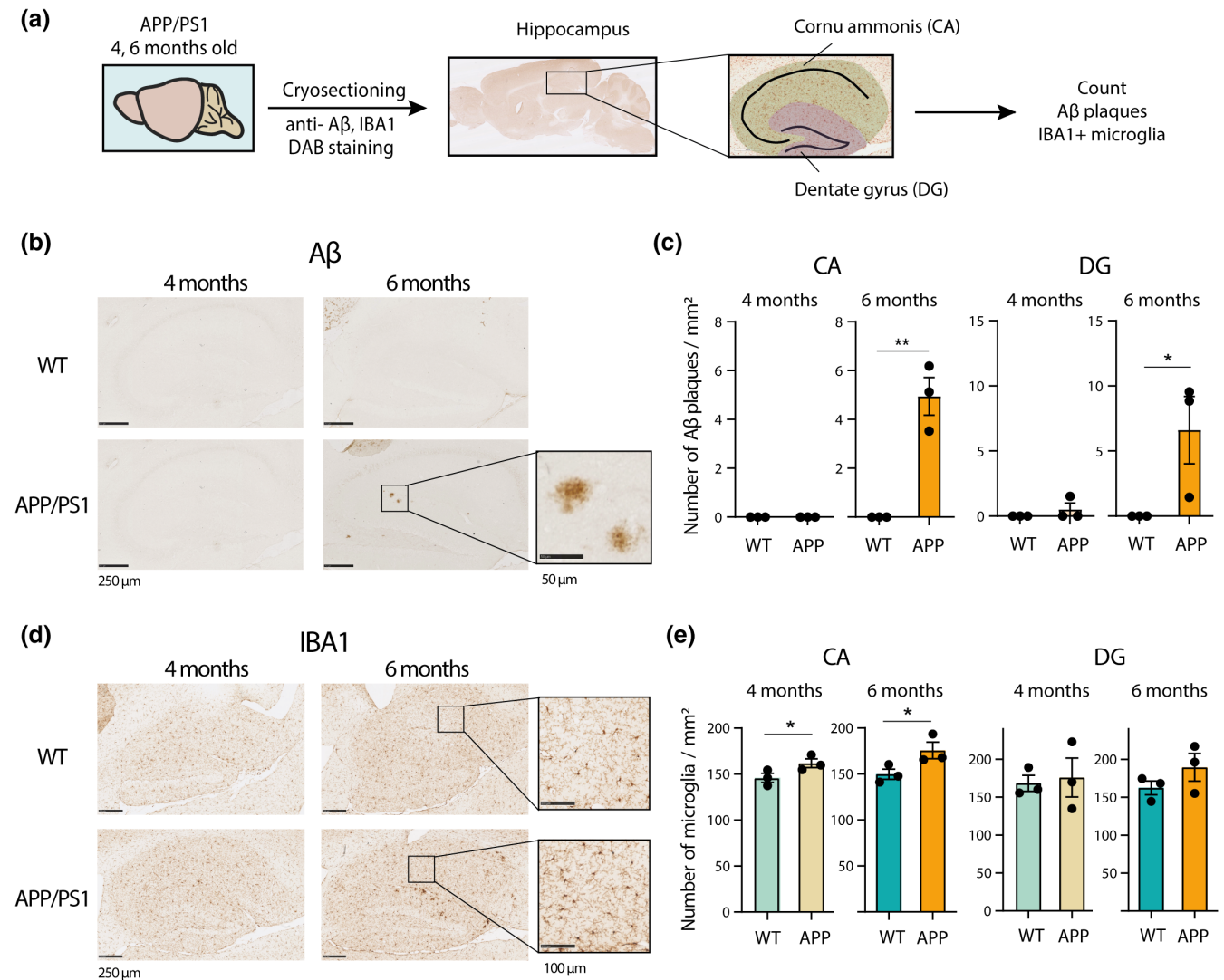


FIGURE 1 Staining of A β and microglia in hippocampi of 4- and 6-month-old APP/PS1 and WT mice. (a) Experimental workflow indicating the use of sagittal sections of PFA-fixed brains from 4- and 6-month-old APP/PS1 and WT mice stained with anti-A β and anti-IBA1 antibodies followed by counting of A β plaques and microglia in CA and DG in the hippocampus. (b) Representative images of A β staining of 4- and 6-month-old APP/PS1 and WT mice (a scale bar of 250 μ m and a scale bar of 50 μ m). (c) Bar plots depicting the number of A β plaques per mm² in 4- and 6-month-old APP/PS1 and WT mice in CA and DG regions. (d) Representative IBA1 staining images of 4- and 6-month-old APP/PS1 and WT mice (a scale bar of 250 μ m and a scale bar of 100 μ m). (e) Bar plots depicting the number of microglia per mm² in 4- and 6-month-old APP/PS1 and WT mice in CA and DG regions. $n=3$ animals per group. Error bars indicate mean \pm SEM. * $p < .05$, ** $p < .01$.

At the age of 6 months, two upregulated genes in APP/PS1 mice (*Cst7*, *Baiap2l2*) were detected (Figure 2c). *Cst7* is associated with phagocytosis and lipid metabolism, and *Baiap2l2* gene is related to vesicle formation. Upregulation of both *Cst7* and *Baiap2l2* genes was previously observed in microglia in 5xFAD AD model mice (Griciuc et al., 2019). These genes might reflect initial transcriptional changes in microglia in response to amyloid. Twenty-one genes, which were more abundantly expressed in 9-month-old APP/PS1 microglia, are all known disease-associated microglia (DAMs) or primed microglia signature genes (Chen et al., 2020; Holtman et al., 2015; Keren-Shaul et al., 2017; Krasemann et al., 2017; Li et al., 2019; Safaiyan et al., 2021) (Figure 2c). For some of these genes, although not significant, an increase in gene expression was already observed in microglia of 6-month-old APP/PS1 mice (Figure 2d). The results indicate

that by bulk RNA-seq of microglia, the first transcriptomic changes in APP/PS1 mice were detected around the age of 6 months, and that many genes that were significantly increased in microglia from 9-month-old APP/PS1 mice already showed signs of dysregulation at 6 months.

3.3 | DAMs were enriched in CD11c^{pos} microglia

By expression profiling of microglia using bulk RNA-seq, the average gene expression profile is determined. This potentially precludes the detection of transcriptomic changes in relatively small subpopulations of microglia. In a previous study, high expression of CD11c (*Itgax* gene) was selectively increased in microglia around A β plaques

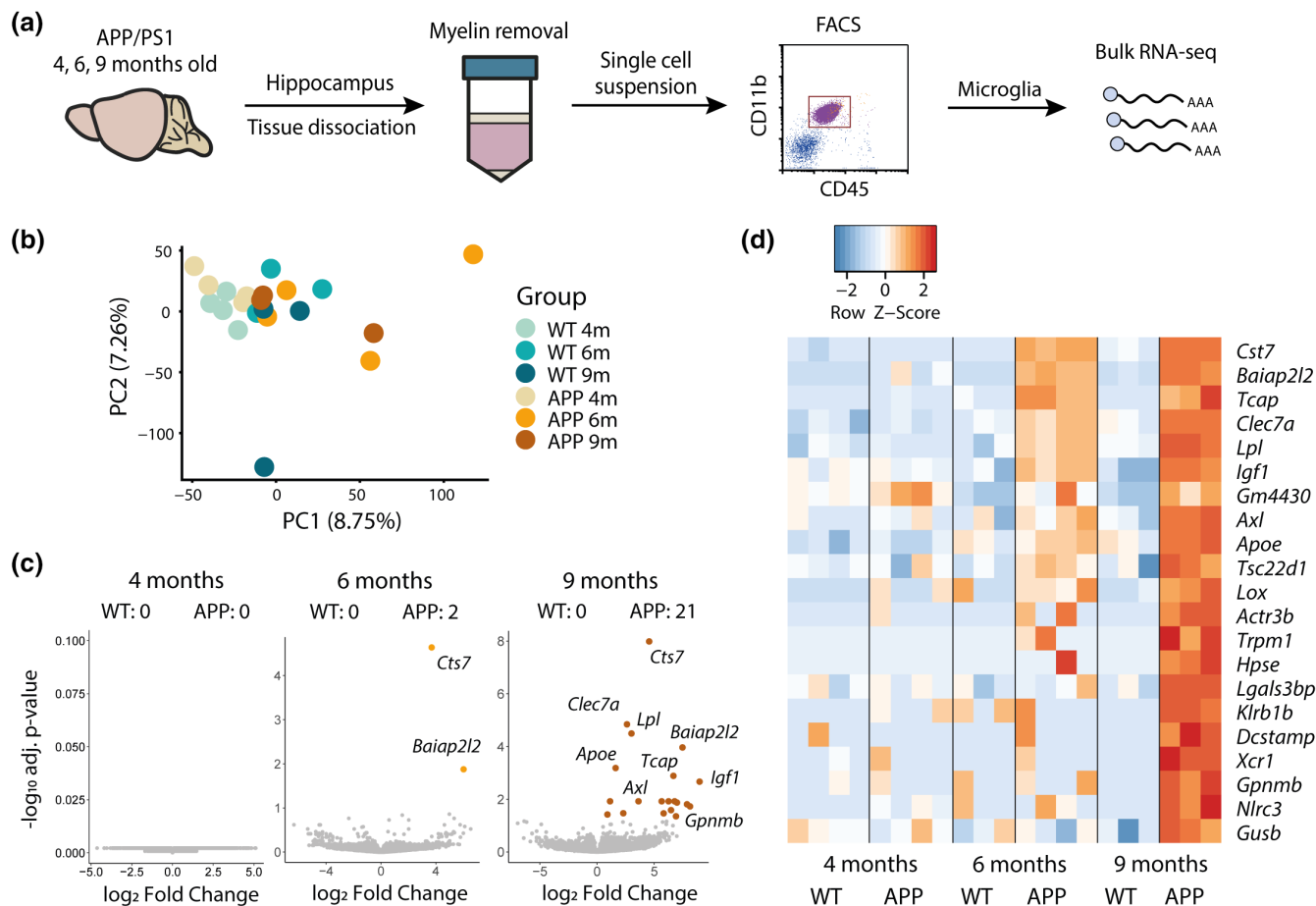


FIGURE 2 Bulk RNA-seq of microglia in hippocampi of 4-, 6-, and 9-month-old APP/PS1 and WT mice. (a) Experimental workflow showing that microglia were isolated from hippocampi of 4-, 6-, and 9-month-old APP/PS1 and WT mice by FACS after tissue dissociation and myelin removal, and bulk RNA-seq was performed. (b) Principal component analysis (PCA) of gene expression profiles of microglia. Colors indicate each group ($n=3$ or 4 animals per group). The x- and y-axes represent the first and second principal components (PC1 and PC2), respectively. (c) Volcano plots depicting differentially expressed genes (DEGs) with colors (LFC > 0, adjusted p value < .05) in the comparisons between APP/PS1 and WT in 4 months (left), 6 months (middle) and 9 months (right). (d) A heat map depicting gene expression of 21 DEGs found in the comparison of APP/PS1 and WT in 9 months. Colors indicate row z-scores in each gene.

in APP/PS1 mice at the age of 9 months (Kamphuis et al., 2016). This subset of microglia was also detected in single-cell/nucleus transcriptomic studies of other amyloid mouse models and post-mortem brains from AD patients, and the proportion of CD11c^{pos} microglia is associated with increasing disease severity (Gerrits et al., 2021; Keren-Shaul et al., 2017). To determine whether this increase in CD11c^{pos} microglia already occurred at 6 months in APP/PS1 mice, we added CD11c to our CD11b/CD45 FACS panel and examined the proportion of CD11c^{pos} cells in the CD11b^{pos}/CD45^{pos} microglia population in the hippocampus and cortex from another cohort (Figures 3a and S3). The proportion of CD11c^{pos} microglia was increased in both the cortex and hippocampus of 6-month-old APP/PS1 mice and accounted for approximately 2% of microglia (Figure 3b). These data indicate that the bulk RNA-seq data likely did not detect the full spectrum of transcriptomic changes in this subpopulation of microglia.

To investigate the transcriptomic profiles of CD11c^{pos} microglia in 6-month-old APP/PS1, we sorted the CD11c^{pos} microglia from

APP/PS1 mice by FACS and performed single-cell RNA sequencing (scRNA-seq) on these microglia populations. After filtering, 2528 microglia (a median of 18,977 UMIs and 789 unique genes per cell) were analyzed and depicted in Uniform Manifold Approximation and Projection (UMAP) plots (Figure 3c,d). CD11c^{pos} microglia showed a different gene expression profile compared to CD11c^{neg} microglia (Figure 3c). Moreover, we observed a transcriptionally distinct microglia population specific to the cortex (Figure 3d). Next, we performed unsupervised clustering of all microglia and identified eight microglia subtypes with different gene-expression profiles (Figure 3e, Table S3). Clusters HOM_1, HOM_2 and HOM_3 were enriched for homeostatic microglia genes (*P2ry12*, *Tmem119*, *Cx3cr1*), and clusters CD11c_1 and CD11c_2 were enriched for DAM signature genes (*Cst7*, *Lpl*, *Apoe*) and depleted for homeostatic microglia genes (Figure 3f). Microglia in the PROLIF cluster highly expressed genes associated with cell proliferation (*Top2a* and *Mki67*), and cluster MONO/MACRO contained cells abundantly expressing marker genes of monocytes and macrophages (*Mrc1* and

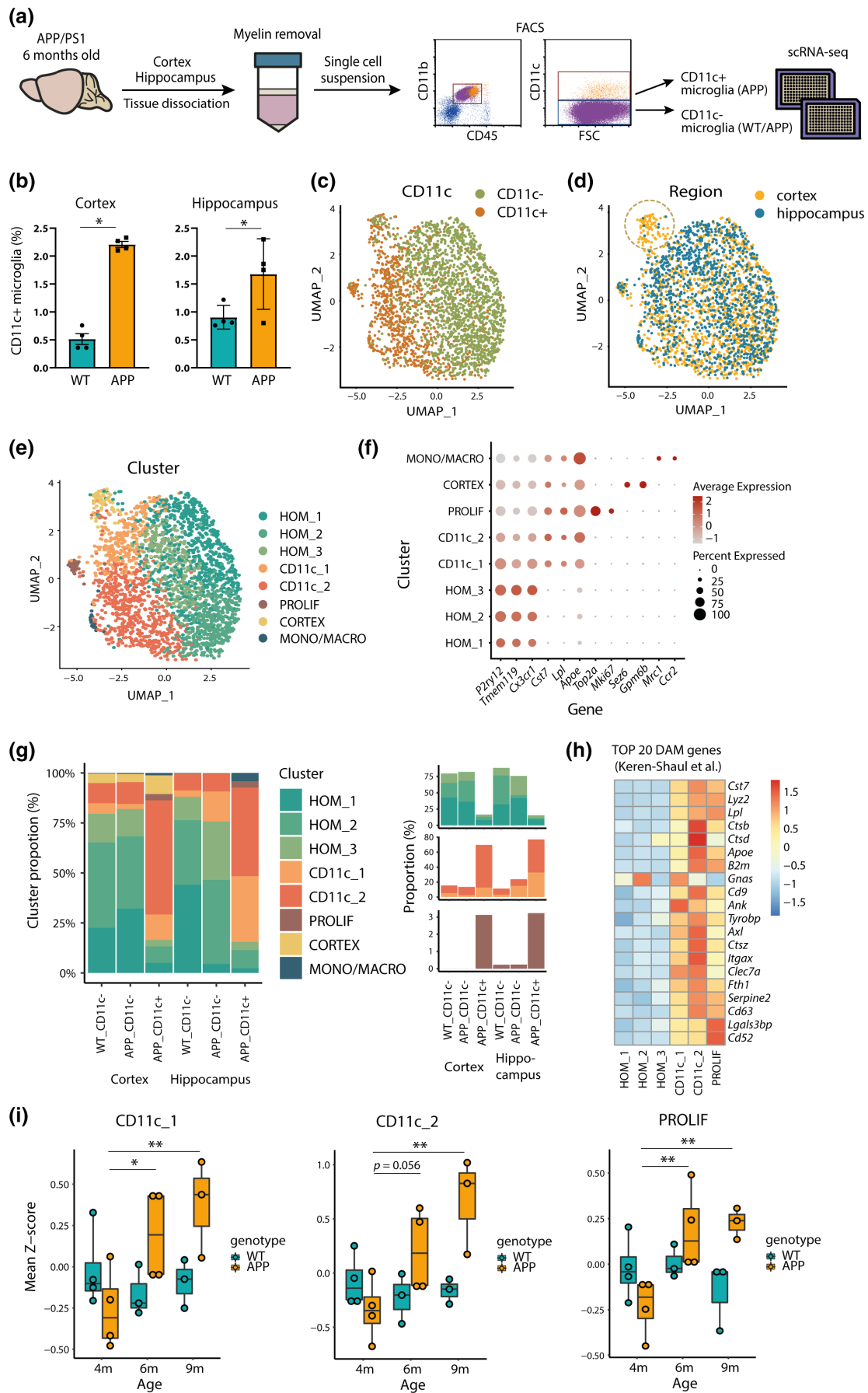


FIGURE 3 scRNA-seq of CD11c^{POS} and CD11c^{NEG} microglia in 6-month-old APP/PS1 and WT mice. (a) Microglia were isolated from cortex and hippocampi of 6-month-old APP/PS1 and WT mice by FACS after tissue dissociation and myelin removal, and single-cell RNA-seq was performed for the CD11c^{POS} (CD11c+) and CD11c^{NEG} (CD11c-) microglia. (b) Bar plots depicting the proportion of CD11c^{POS} microglia in cortex and hippocampi. (c–e) Uniform Manifold Approximation and Projection (UMAP) depicting all individual cells with corresponding colors of CD11c^{NEG} or CD11c^{POS} microglia (c), microglia from cortex or hippocampi (d) and eight different clusters (e). (f) A dot plot depicting the expression of marker genes in each cluster. Colors indicate z-score of expression of the genes among the clusters. Diameter of the dots indicates the percentage of cells expressing the genes. (g) Bar plots depicting the proportions of each cluster in each condition. Colors indicate the clusters. (h) A heat map depicting the expression of the TOP 20 DAM genes from Keren-Shaul et al. in each cluster. Colors indicate z-score of expression the genes among the clusters. (i) Box plots depicting the mean of z-score of marker genes (CD11c_1, CD11c_2, and PROLIF) in the bulk RNA-seq data. Boxes are from the first quartile to the third quartile, and lines indicate the median. *n* = 4 animals per group. **p* < .05, ***p* < .01.

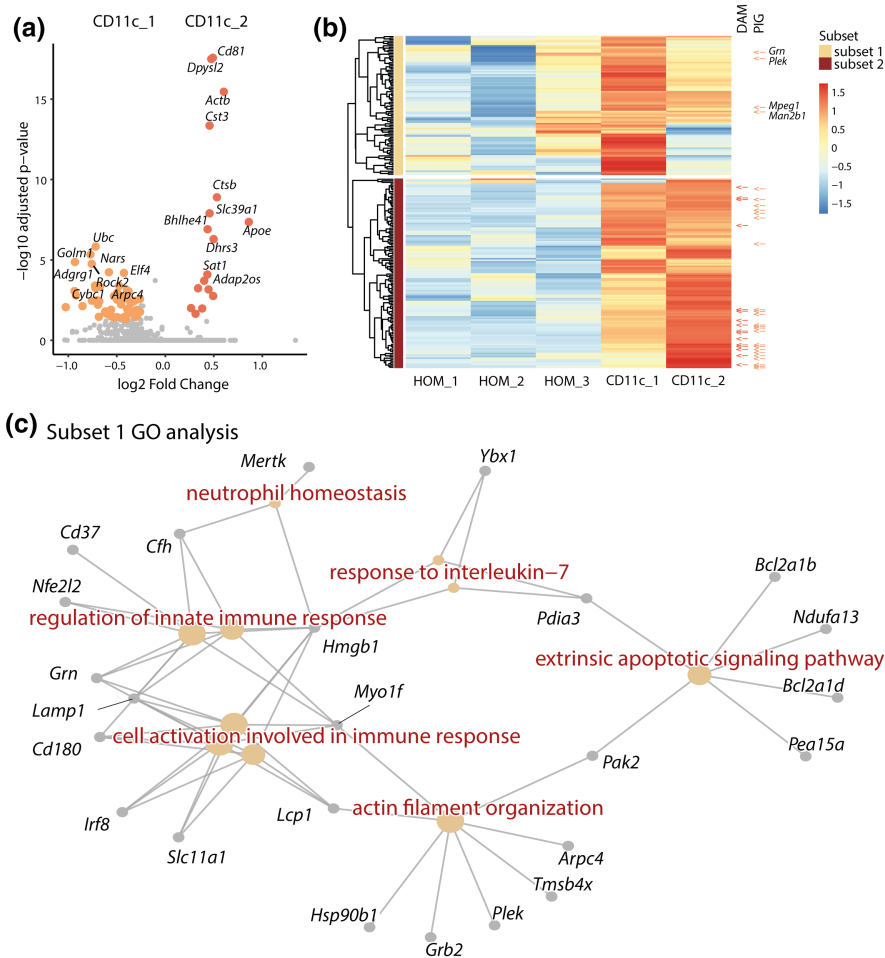


FIGURE 4 Differentially expressed genes between CD11c_1 and CD11c_2 clusters. (a) A volcano plot depicting the result of DEG analysis (LFC > .25, adjusted *p*-value < .05) between the CD11c_1 and CD11c_2 clusters. (b) A heat map depicting gene expression of marker genes of the CD11c_1 and CD11c_2 clusters with a hierarchical clustering of the genes based on their expression pattern among the 5 clusters (HOM_1, HOM_2, HOM_3, CD11c_1, and CD11c_2). Colors indicate row z-scores in each gene. The genes overlapping with TOP20 DAM genes from Keren-Shaul et al., 2017 and PIGs from Chen et al., 2020 were also shown. (c) A cnetplot depicting the result of gene ontology analysis (TOP10 enriched functions) of the genes in cluster 2 and the genes associated with the functions.

Ccr2) (Figure 3f). Cluster CORTEX was exclusively derived from cortex samples, with a distinct expression profile enriched for genes typically associated with neurons and synapses (Figure S4a,b). Gene ontology analysis indicated these genes were associated with neuronal functions such as learning, memory, cognition, and synapse organization (Figure S4c). Synaptic GO analysis with SynGo confirmed the enrichment of synaptic functions, and some of the

detected genes encode pre- and post-synaptic proteins (Figure S4d, Table S4), while for other microglia clusters, no enrichment of synaptic GO terms was observed. Some genes associated with phagocytosis and lysosome such as *Clec7a* and *Cst7* were also highly expressed in the CORTEX cluster (Figure S4e).

CD11c^{NEG} microglia, from both WT and APP/PS1 mice, primarily contributed to the homeostatic clusters (HOM_1, HOM_2, and

HOM_3), and CD11c^{POS} microglia from APP/PS1 mice were enriched in the CD11c_1, CD11c_2, and PROLIF clusters (Figure 3g). Interestingly, microglia in the PROLIF cluster were also enriched for DAM marker genes, suggesting that the PROLIF cluster is a subset of proliferating DAMs (Figure 3h). Thus, these data suggest that most of the CD11c^{POS} microglia expressed a DAM gene signature. Since we analyzed microglia of mice of several ages in the bulk RNA-seq experiment (Figure 2a), we examined the expression of CD11c_1, CD11c_2, and PROLIF clusters marker genes (Figure S4a) over time in APP/PS1 microglia. The average expression of the marker genes of these clusters was increased in APP/PS1 microglia with progressing age (Figure 3i).

3.4 | Genes associated with the transition from homeostatic microglia to DAMs

To investigate the difference between microglia in the CD11c_1 and CD11c_2 clusters, we compared the genes expressed in these clusters. DAM marker genes, such as *Apoe* and *Ctsb*, were most abundantly expressed in the CD11c_2 cluster and less in the CD11c_1 cluster (Figure 4a), indicating that CD11c_1 microglia were at an earlier stage of the homeostatic to DAM transition than CD11c_2 microglia. To determine which genes were involved in the early transition from homeostatic to DAMs, the CD11c_1 and CD11c_2 cluster marker genes were classified by hierarchical clustering based on their expression in the HOM_1, HOM_2, HOM_3, CD11c_1, and CD11c_2 clusters. This resulted in two different subsets of genes (Figure 4b, Table S5) where genes in subset 2 included many DAM marker genes and were highly expressed in the CD11c_2 cluster. By contrast, the genes in subset 1 contained no DAM markers and were highly expressed in the CD11c_1 and HOM_3 clusters. This suggests that subset 1 genes are involved in the early changes from homeostatic microglia to DAMs (Figure 4b). Gene ontology analysis of the genes in subset 1 showed that these genes were associated with cell activation in immune responses, apoptotic signaling pathway, and actin filament organization (Figure 4c). The genes in subset 1 include *Irf8*, a transcription factor with crucial roles in myeloid cell maturation and activation (Tamura et al., 2000), and *Grn*, *Man2b1*, *Plek*, and *Mpeg1*, which were previously identified as A β plaque-induced genes (PIGs) in another AD mouse model (*App*^{NL-G-F}) (Chen et al., 2020). To investigate whether these genes are also enriched in plaque-distant microglia in APP/PS1 mice, we compared the 91 genes of subset 1 with the previously reported 87 genes enriched in plaque-distant microglia (Hemonnot-Girard et al., 2022). An overlap of seven genes between these two gene lists was observed, including *Irf8* and *Grn*, suggesting these genes might be early markers of microglia HOM-DAM transition. In summary, here we identified the genes in microglia of which the expression levels were affected early on in response to A β in APP/PS1 mice.

4 | DISCUSSION

In this study, microglial gene expression analyses were performed to delineate the early changes in microglia in response to amyloid in APP/PS1 mice. By bulk RNA-seq, the first transcriptomic changes in hippocampal microglia were detected in 6-month-old APP/PS1 mice. The differentially expressed genes that were enriched in 6- and 9-month-old APP/PS1 mice were previously reported as DAMs or primed microglia signature genes (Chen et al., 2020; Holtman et al., 2015; Keren-Shaul et al., 2017; Krasemann et al., 2017; Li et al., 2019; Safaiyan et al., 2021). We detected no differentially expressed genes in 4-month-old APP/PS1 mice by bulk RNA-seq. Microglia density was increased at that age, and gliosis with CD68 expression was observed in 4-month-old APP/PS1 mice before A β plaques were detected in the hippocampus in our previous study (Kater et al., 2023). We hypothesized that a small population of microglia changed their phenotype in response to soluble A β with potentially subtle transcriptomic changes. This might have precluded the detection of differentially expressed genes by bulk RNA-seq in microglia from 4-month-old APP/PS1 mice, which measures the average gene expression of all isolated microglia.

In previous studies with 9-month-old APP/PS1 mice, CD11c^{POS} microglia were reported to emerge in response to amyloid (Kamphuis et al., 2016). The gene expression profile of this microglia subset was assessed here by scRNA-seq, and we identified three clusters (CD11c_1, CD11c_2, and PROLIF), in which CD11c^{POS} microglia were enriched. Among these clusters, microglia in the CD11c_2 cluster exhibited a gene expression pattern most similar to previously reported DAMs (Keren-Shaul et al., 2017). Microglia in the CD11c_1 cluster were likely at an earlier state along the homeostatic microglia to DAM transition trajectory than the CD11c_2 cluster microglia, as their gene expression signature was an intermediate between the homeostatic and CD11c_2 microglia. By investigating the transcriptional trajectory from homeostatic to CD11c_2 microglia, we identified a new set of genes, enriched in the HOM_3 and CD11c_1 cluster, which is distinct from known DAM genes and these genes are likely involved in the early transition from homeostatic microglia to DAMs. The HOM-DAM transition genes were associated with innate immune responses, and cytoskeletal processes suggesting morphological alterations. Genes involved in cell activation in immune responses included *Irf8* and *Grn*, which were also enriched in plaque-distant microglia in APP/PS1 mice (Hemonnot-Girard et al., 2022), suggesting these genes might be early markers of microglia HOM-DAM transition. *Irf8* encodes IRF8, a transcription factor of the interferon regulatory factor (IRF) family. IRF8 has important roles in microglia development and their motility (Kierdorf et al., 2013; Masuda et al., 2014), and also in transforming microglia into a reactive state (Masuda et al., 2012; Zhou et al., 2019). In addition, another study reported that A β ₁₋₄₀-induced microglial activation in an IRF8-dependent manner in Tg2576 amyloid mice (Zeng et al., 2017). *Grn*, *Man2b1*, *Plek*, and *Mpeg1* were previously

identified as plaque-induced genes (PIGs), with high gene expression around A β plaques in another AD mouse model (*App*^{NL-G-F}) (Chen et al., 2020). In particular, *Grn*, which encodes the secreted glycoprotein Progranulin (PGRN), plays an important role in modulating inflammatory activation of microglia through reducing excessive lysosomal activation (Tanaka et al., 2013). In homozygous *Grn*-deficient mice, microglia showed exaggerated inflammation and cytotoxicity (Yin et al., 2010). Genetic mutations in *Grn* have been identified as a cause of frontotemporal lobar degeneration (FTLD) (Baker et al., 2006; Cruts et al., 2006), but single-nucleus RNA sequencing (snRNA-seq) of post-mortem cortex tissue of FTLD patients with *GRN* mutations revealed that transcriptomic profiles of microglia and macrophages were not affected compared to control patients (Gerrits et al., 2022). In human AD cases and AD model mice, increased expression of PGRN was observed in microglia (Mendsaikhani et al., 2019). A study with 6-month-old *Grn*-deficient APP/PS1 mice showed increased CD68 expression in microglia around plaques and upregulation of DAM genes, including *Trem2* and *Tyrobp* (Takahashi et al., 2017), suggesting PGRN in microglia is involved in the transition from homeostatic microglia to DAMs. Altogether, these findings suggest that the novel subset 1 genes enriched in the HOM_3 and CD11c_1 cluster, including *Irf8* and *Grn*, regulate the early transition from homeostatic microglia to DAMs reacting to A β .

Microglia in the CORTEX cluster were enriched for genes mostly expressed in neurons, which was also observed in a previous study with human fetal microglia (Kracht et al., 2020). Chromatin accessibility profiles of these fetal microglia revealed that the promoter regions of these neuronal genes were closed, suggesting these genes were not expressed by microglia. In this context, it is of interest to note that the CORTEX transcriptome is enriched for synaptic genes as established by SynGO (Koopmans et al., 2019) analysis (Figure S4d and Table S4). Synaptic transcripts form a separate pool that is to large extent independent of somal transcription (Holt et al., 2019). Synaptic transcripts encoding both pre- and post-synaptic proteins (e.g. including calmodulin-kinase II and NMDA receptor subunits), together with *Clec7a* and *Cst7*, the latter of which are associated with phagocytosis and lysosome, were highly expressed in the CORTEX cluster. This suggest that these microglia phagocytose synapses, accounting for these transcripts in microglia. However, why transcripts encoding synaptic proteins are specifically enriched in cortical microglia is currently unclear.

Our study has certain limitations that should be acknowledged. First, the number of cells analyzed in our smart-seq2-based scRNA-seq. A higher number of cells would have allowed us to achieve higher resolution in clustering of microglia subtypes, and to perform more comprehensive trajectory analyses. However, due to the relatively low number of CD11c^{POS} microglia in 6-month-old APP/PS1 mice, it would have required a high number of mice to obtain a sufficiently high number of CD11c^{POS} cells. Additionally, we only were able to use male APP/PS1 mice, which was due to litter compositions, which we could not influence. As

a result, we currently lack information regarding potential sex differences in microglial response to A β at early stages. Further research exploring the role of sex in microglial dynamics and the response to A β would be necessary to gain a more comprehensive understanding of sex-dependent differences. Furthermore, in this study, we performed immunohistochemical analyses and bulk RNA sequencing only on microglia in the hippocampus. The single cell RNA-seq analysis included microglia in the cortex and the transcriptomic profile of microglia was similar to the one in the hippocampus. Therefore, we do not expect a lot of difference between cortex and hippocampus. However, the difference of microglial response to amyloid in different brain regions is an interesting topic to be explored.

Taken together, by performing RNA sequencing and investigating the transcriptional trajectory of microglia in APP/PS1 mice, we determined the earliest transcriptional changes in microglia in response to A β . We identified a set of inflammation-associated genes that was transiently increased during the early transition from homeostatic microglia to DAMs, leading to a better understanding of the initial transcriptional changes that occur in microglia triggered by A β that precede the DAM gene signature. To further elucidate the detailed mechanisms underlying the transition from homeostatic microglia to DAMs, additional investigation is needed, which could lead to the development of novel therapeutic strategies that specifically target the early stages of AD by modulating neuroinflammation.

DECLARATION OF TRANSPARENCY

The authors, reviewers and editors affirm that in accordance to the policies set by the *Journal of Neuroscience Research*, this manuscript presents an accurate and transparent account of the study being reported and that all critical details describing the methods and results are present.

AUTHOR CONTRIBUTIONS

Conceptualization, B.J.L.E., E.W.G.M.B., E.M.H., J.M., A.B.S., and M.H.G.V.; *Methodology*, B.J.L.E. and T.O.; *Resources*, M.K., and C.F.M.H.; *Investigation*, T.O. and E.M.W.; *Writing—Original Draft*, T.O. and B.J.L.E.; *Writing—Review & Editing*, E.W.G.M.B., E.M.H., J.M., A.B.S., M.H.G.V., M.K., and C.F.M.H.; *Visualization*, T.O.; *Supervision*, B.J.L.E.; *Funding Acquisition*, B.J.L.E., E.W.G.M.B., E.M.H., J.M., A.B.S., and M.H.G.V.

ACKNOWLEDGMENTS

The authors would like to thank Nieske Brouwer and Qiong Jiang for assistance with microglia isolation and library preparations for sequencing, Geert Mesander, Johan Teunis and Theo Bijma of the Flow Cytometry Unit (FCU) at University Medical Center Groningen (UMCG) for FACS support, Diana Spierings, Jennefer Beenen, and Victor Guryev of the Research Sequencing Facility at European Research Institute for the Biology of Aging (ERIBA) for generating and processing sequencing data, Astrid Alsema and Emma Gerrits for the initial processing of single-cell RNA-seq data.

FUNDING INFORMATION

This work was supported by a Memorabel-ZonMw grant (73305 0816).

CONFLICT OF INTEREST STATEMENT

The authors declare no potential conflict of interest.

PEER REVIEW

The peer review history for this article is available at <https://www.webofscience.com/api/gateway/wos/peer-review/10.1002/jnr.25295>.

DATA AVAILABILITY STATEMENT

All the sequencing data are available at NCBI GEO (accession number GSE226939, link: <https://www.ncbi.nlm.nih.gov/geo/query/acc.cgi?acc=GSE226939>).

ORCID

Takuya Oshima  <https://orcid.org/0000-0002-1430-4211>

Mandy S. J. Kater  <https://orcid.org/0000-0003-4832-2597>

Christiaan F. M. Huffels  <https://orcid.org/0000-0002-9070-3644>

Mark H. G. Verheijen  <https://orcid.org/0000-0002-3739-3755>

Bart J. L. Eggen  <https://orcid.org/0000-0001-8941-0353>

REFERENCES

- Alsema, A. M., Jiang, Q., Kracht, L., Gerrits, E., Dubbelaar, M. L., Miedema, A., Brouwer, N., Hol, E. M., Middeldorp, J., van Dijk, R., Woodbury, M., Wachter, A., Xi, S., Möller, T., Biber, K. P., Kooistra, S. M., Boddeke, E. W. G. M., & Eggen, B. J. L. (2020). Profiling microglia from Alzheimer's disease donors and non-demented elderly in acute human postmortem cortical tissue. *Frontiers in Molecular Neuroscience*, 13, 134. <https://doi.org/10.3389/fnmol.2020.00134>
- Alzheimer's Association. (2022). 2022 Alzheimer's disease facts and figures. *Alzheimer's & Dementia*, 18(4), 700–789. <https://doi.org/10.1002/alz.12638>
- Baker, M., Mackenzie, I. R., Pickering-Brown, S. M., Gass, J., Rademakers, R., Lindholm, C., Snowden, J., Adamson, J., Sadovnick, A. D., Rollinson, S., Cannon, A., Dwosh, E., Neary, D., Melquist, S., Richardson, A., Dickson, D., Berger, Z., Eriksen, J., Robinson, T., ... Hutton, M. (2006). Mutations in progranulin cause tau-negative frontotemporal dementia linked to chromosome 17. *Nature*, 442(7105), 916–919. <https://doi.org/10.1038/nature05016>
- Campion, D., Flaman, J.-M., Brice, A., Hannequin, D., Dubois, B., Martin, C., Moreau, V., Charbonnier, F., Didierjean, O., Tardieu, S., Penet, C., Puel, M., Pasquier, F., Le Doze, F., Bellis, G., Calenda, A., Heilig, R., Martinez, M., Mallet, J., ... Frebourg, T. (1995). Mutations of the presenilin 1 gene in families with early-onset Alzheimer's disease. *Human Molecular Genetics*, 4(12), 2373–2377. <https://doi.org/10.1093/hmg/4.12.2373>
- Chen, W.-T., Lu, A., Craessaerts, K., Pavie, B., Sala Frigerio, C., Corthout, N., Qian, X., Laláková, J., Kühnemund, M., Voytyuk, I., Wolfs, L., Mancuso, R., Salta, E., Balusu, S., Snellinx, A., Munck, S., Jurek, A., Fernandez Navarro, J., Saido, T. C., ... De Strooper, B. (2020). Spatial transcriptomics and in situ sequencing to study Alzheimer's disease. *Cell*, 182(4), 976–991.e19. <https://doi.org/10.1016/j.cell.2020.06.038>
- Cribbs, D. H., Berchtold, N. C., Perreau, V., Coleman, P. D., Rogers, J., Tenner, A. J., & Cotman, C. W. (2012). Extensive innate immune gene activation accompanies brain aging, increasing vulnerability to cognitive decline and neurodegeneration: A microarray study. *Journal of Neuroinflammation*, 9(1), 643. <https://doi.org/10.1186/1742-2094-9-179>
- Cruts, M., Gijselinck, I., van der Zee, J., Engelborghs, S., Wils, H., Pirici, D., Rademakers, R., Vandenbergh, R., Dermaut, B., Martin, J.-J., van Duijn, C., Peeters, K., Sciot, R., Santens, P., De Pooter, T., Mattheijssens, M., Van den Broeck, M., Cuijt, I., Vennekens, K., ... Van Broeckhoven, C. (2006). Null mutations in progranulin cause ubiquitin-positive frontotemporal dementia linked to chromosome 17q21. *Nature*, 442(7105), 920–924. <https://doi.org/10.1038/nature05017>
- DeTure, M. A., & Dickson, D. W. (2019). The neuropathological diagnosis of Alzheimer's disease. *Molecular Neurodegeneration*, 14(1), 32. <https://doi.org/10.1186/s13024-019-0333-5>
- Galatro, T. F., Holtman, I. R., Lerario, A. M., Vainchtein, I. D., Brouwer, N., Sola, P. R., Veras, M. M., Pereira, T. F., Leite, R. E. P., Möller, T., Wes, P. D., Sogayar, M. C., Laman, J. D., den Dunnen, W., Pasqualucci, C. A., Oba-Shinjo, S. M., Boddeke, E. W. G. M., Marie, S. K. N., & Eggen, B. J. L. (2017). Transcriptomic analysis of purified human cortical microglia reveals age-associated changes. *Nature Neuroscience*, 20(8), 1162–1171. <https://doi.org/10.1038/nn.4597>
- Gerrits, E., Brouwer, N., Kooistra, S. M., Woodbury, M. E., Vermeiren, Y., Lambourne, M., Mulder, J., Kummer, M., Möller, T., Biber, K., den Dunnen, W. F. A., De Deyn, P. P., Eggen, B. J. L., & Boddeke, E. W. G. M. (2021). Distinct amyloid- β and tau-associated microglia profiles in Alzheimer's disease. *Acta Neuropathologica*, 141(5), 681–696. <https://doi.org/10.1007/s00401-021-02263-w>
- Gerrits, E., Giannini, L. A. A., Brouwer, N., Melhem, S., Seilhean, D., Le Ber, I., Kamermans, A., Kooij, G., de Vries, H. E., Boddeke, E. W. G. M., Seelaar, H., van Swieten, J. C., & Eggen, B. J. L. (2022). Neurovascular dysfunction in GRN-associated frontotemporal dementia identified by single-nucleus RNA sequencing of human cerebral cortex. *Nature Neuroscience*, 25(8), 1034–1048. <https://doi.org/10.1038/s41593-022-01124-3>
- Goate, A., Chartier-Harlin, M.-C., Mullan, M., Brown, J., Crawford, F., Fidani, L., Giuffra, L., Haynes, A., Irving, N., James, L., Mant, R., Newton, P., Rooke, K., Roques, P., Talbot, C., Pericak-Vance, M., Roses, A., Williamson, R., Rossor, M., ... Hardy, J. (1991). Segregation of a missense mutation in the amyloid precursor protein gene with familial Alzheimer's disease. *Nature*, 349(6311), 704–706. <https://doi.org/10.1038/349704a0>
- Griciuc, A., Patel, S., Federico, A. N., Choi, S. H., Innes, B. J., Oram, M. K., Cereghetti, G., McGinty, D., Anselmo, A., Sadreyev, R. I., Hickman, S. E., El Khoury, J., Colonna, M., & Tanzi, R. E. (2019). TREM2 acts downstream of CD33 in modulating microglial pathology in Alzheimer's disease. *Neuron*, 103(5), 820–835.e7. <https://doi.org/10.1016/j.neuron.2019.06.010>
- Hao, Y., Hao, S., Andersen-Nissen, E., Mauck, W. M., Zheng, S., Butler, A., Lee, M. J., Wilk, A. J., Darby, C., Zager, M., Hoffman, P., Stoeckius, M., Papalexi, E., Mimitou, E. P., Jain, J., Srivastava, A., Stuart, T., Fleming, L. M., Yeung, B., ... Satija, R. (2021). Integrated analysis of multimodal single-cell data. *Cell*, 184(13), 3573–3587.e29. <https://doi.org/10.1016/j.cell.2021.04.048>
- Hemonnot-Girard, A.-L., Meersseman, C., Pastore, M., Garcia, V., Linck, N., Rey, C., Chebbi, A., Jeanneteau, F., Ginsberg, S. D., Lachuer, J., Reynes, C., Rassendren, F., & Hirbec, H. (2022). Comparative analysis of transcriptome remodeling in plaque-associated and plaque-distant microglia during amyloid- β pathology progression in mice. *Journal of Neuroinflammation*, 19(1), 234. <https://doi.org/10.1186/s12974-022-02581-0>
- Holt, C. E., Martin, K. C., & Schuman, E. M. (2019). Local translation in neurons: Visualization and function. *Nature Structural & Molecular Biology*, 26(7), 557–566. <https://doi.org/10.1038/s41594-019-0263-5>
- Holtman, I. R., Raj, D. D., Miller, J. A., Schaafsma, W., Yin, Z., Brouwer, N., Wes, P. D., Möller, T., Orre, M., Kamphuis, W., Hol, E. M., Boddeke, E. W.

- G. M., & Eggen, B. J. L. (2015). Induction of a common microglia gene expression signature by aging and neurodegenerative conditions: A co-expression meta-analysis. *Acta Neuropathologica Communications*, 3(1), 31. <https://doi.org/10.1186/s40478-015-0203-5>
- Jankowsky, J. L., Slunt, H. H., Gonzales, V., Jenkins, N. A., Copeland, N. G., & Borchelt, D. R. (2004). APP processing and amyloid deposition in mice haplo-insufficient for presenilin 1. *Neurobiology of Aging*, 25(7), 885–892. <https://doi.org/10.1016/j.neurobiolaging.2003.09.008>
- Jansen, I. E., Savage, J. E., Watanabe, K., Bryois, J., Williams, D. M., Steinberg, S., Sealock, J., Karlsson, I. K., Hägg, S., Athanasiu, L., Voyle, N., Proitsi, P., Witoelar, A., Stringer, S., Aarsland, D., Almdahl, I. S., Andersen, F., Bergh, S., Bettella, F., ... Posthuma, D. (2019). Genome-wide meta-analysis identifies new loci and functional pathways influencing Alzheimer's disease risk. *Nature Genetics*, 51(3), 404–413. <https://doi.org/10.1038/s41588-018-0311-9>
- Kamphuis, W., Kooijman, L., Schettters, S., Orre, M., & Hol, E. M. (2016). Transcriptional profiling of CD11c-positive microglia accumulating around amyloid plaques in a mouse model for Alzheimer's disease. *Biochimica et Biophysica Acta—Molecular Basis of Disease*, 1862(10), 1847–1860. <https://doi.org/10.1016/j.bbadis.2016.07.007>
- Kater, M. S. J., Huffels, C. F. M., Oshima, T., Renckens, N. S., Middeldorp, J., Boddeke, E. W. G. M., Smit, A. B., Eggen, B. J. L., Hol, E. M., & Verheijen, M. H. G. (2023). Prevention of microglial activation halts early memory loss in a mouse model of Alzheimer's disease. *Brain, Behavior, and Immunity*, 107, 225–241. <https://doi.org/10.1016/j.bbi.2022.10.009>
- Keren-Shaul, H., Spinrad, A., Weiner, A., Matcovitch-Natan, O., Dvir-Szternfeld, R., Ulland, T. K., David, E., Baruch, K., Lara-Astaiso, D., Toth, B., Itzkovitz, S., Colonna, M., Schwartz, M., & Amit, I. (2017). A unique microglia type associated with restricting development of Alzheimer's disease. *Cell*, 169(7), 1276–1290.e17. <https://doi.org/10.1016/j.cell.2017.05.018>
- Kierdorf, K., Erny, D., Goldmann, T., Sander, V., Schulz, C., Perdiguero, E. G., Wieghofer, P., Heinrich, A., Riemke, P., Hölscher, C., Müller, D. N., Luckow, B., Brouwer, T., Debowski, K., Fritz, G., Opendakker, G., Diefenbach, A., Biber, K., Heikenwalder, M., ... Prinz, M. (2013). Microglia emerge from erythromyeloid precursors via Pu.1- and Irf8-dependent pathways. *Nature Neuroscience*, 16(3), 273–280. <https://doi.org/10.1038/nn.3318>
- Koopmans, F., van Nierop, P., Andres-Alonso, M., Byrnes, A., Cijssouw, T., Coba, M. P., Cornelisse, L. N., Farrell, R. J., Goldschmidt, H. L., Howrigan, D. P., Hussain, N. K., Imig, C., de Jong, A. P. H., Jung, H., Kohansalnodehi, M., Kramarz, B., Lipstein, N., Lovering, R. C., MacGillivray, H., ... Verhage, M. (2019). SynGO: An evidence-based, expert-curated knowledge base for the synapse. *Neuron*, 103(2), 217–234.e4. <https://doi.org/10.1016/j.neuron.2019.05.002>
- Kracht, L., Borggrewe, M., Eskandar, S., Brouwer, N., de Sousa, C., Lopes, S. M., Laman, J. D., Scherjon, S. A., Prins, J. R., Kooistra, S. M., & Eggen, B. J. L. (2020). Human fetal microglia acquire homeostatic immune-sensing properties early in development. *Science*, 369(6503), 530–537. <https://doi.org/10.1126/science.aba5906>
- Krasemann, S., Madore, C., Cialic, R., Baufeld, C., Calcagno, N., El Fatimy, R., Beckers, L., O'Loughlin, E., Xu, Y., Fanek, Z., Greco, D. J., Smith, S. T., Tweet, G., Humulock, Z., Zrzavy, T., Conde-Sanroman, P., Gacias, M., Weng, Z., Chen, H., ... Butovsky, O. (2017). The TREM2-APOE pathway drives the transcriptional phenotype of dysfunctional microglia in neurodegenerative diseases. *Immunity*, 47(3), 566–581.e9. <https://doi.org/10.1016/j.immuni.2017.08.008>
- Law, C. W., Alhamdoosh, M., Su, S., Dong, X., Tian, L., Smyth, G. K., & Ritchie, M. E. (2018). RNA-seq analysis is easy as 1-2-3 with limma, Glimma and edgeR. *F1000Research*, 5, 1408. <https://doi.org/10.12688/f1000research.9005.3>
- Li, Q., Cheng, Z., Zhou, L., Darmanis, S., Neff, N. F., Okamoto, J., Gulati, G., Bennett, M. L., Sun, L. O., Clarke, L. E., Marschallinger, J., Yu, G., Quake, S. R., Wyss-Coray, T., & Barres, B. A. (2019). Developmental heterogeneity of microglia and brain myeloid cells revealed by deep single-cell RNA sequencing. *Neuron*, 101(2), 406363. <https://doi.org/10.1016/j.neuron.2018.12.006>
- Masuda, T., Nishimoto, N., Tomiyama, D., Matsuda, T., Tozaki-Saitoh, H., Tamura, T., Kohsaka, S., Tsuda, M., & Inoue, K. (2014). IRF8 is a transcriptional determinant for microglial motility. *Purinergic Signalling*, 10(3), 515–521. <https://doi.org/10.1007/s11302-014-9413-8>
- Masuda, T., Tsuda, M., Yoshinaga, R., Tozaki-Saitoh, H., Ozato, K., Tamura, T., & Inoue, K. (2012). IRF8 is a critical transcription factor for transforming microglia into a reactive phenotype. *Cell Reports*, 1(4), 334–340. <https://doi.org/10.1016/j.celrep.2012.02.014>
- Mendsaikhan, A., Tooyama, I., & Walker, D. G. (2019). Microglial progranulin: Involvement in Alzheimer's disease and neurodegenerative diseases. *Cell*, 8(3), 230. <https://doi.org/10.3390/cells8030230>
- Morimoto, K., Horio, J., Satoh, H., Sue, L., Beach, T., Arita, S., Tooyama, I., & Konishi, Y. (2011). Expression profiles of cytokines in the brains of Alzheimer's disease (AD) patients compared to the brains of non-demented patients with and without increasing AD pathology. *Journal of Alzheimer's Disease*, 25(1), 59–76. <https://doi.org/10.3233/JAD-2011-101815>
- Plescher, M., Seifert, G., Hansen, J. N., Bedner, P., Steinhäuser, C., & Halle, A. (2018). Plaque-dependent morphological and electrophysiological heterogeneity of microglia in an Alzheimer's disease mouse model. *Glia*, 66(7), 1464–1480. <https://doi.org/10.1002/glia.23318>
- Ritchie, M. E., Phipson, B., Wu, D., Hu, Y., Law, C. W., Shi, W., & Smyth, G. K. (2015). limma powers differential expression analyses for RNA-sequencing and microarray studies. *Nucleic Acids Research*, 43(7), e47. <https://doi.org/10.1093/nar/gkv007>
- Robinson, M. D., McCarthy, D. J., & Smyth, G. K. (2010). edgeR: A Bioconductor package for differential expression analysis of digital gene expression data. *Bioinformatics*, 26(1), 139–140. <https://doi.org/10.1093/bioinformatics/btp616>
- Safaiyan, S., Besson-Girard, S., Kaya, T., Cantuti-Castelvetri, L., Liu, L., Ji, H., Schifferer, M., Gouna, G., Usifo, F., Kannaiyan, N., Fitzner, D., Xiang, X., Rossner, M. J., Brendel, M., Gokce, O., & Simons, M. (2021). White matter aging drives microglial diversity. *Neuron*, 109(7), 1100–1117.e10. <https://doi.org/10.1016/j.neuron.2021.01.027>
- Sala Frigerio, C., Wolfs, L., Fattorelli, N., Thrupp, N., Voytyuk, I., Schmidt, I., Mancuso, R., Chen, W. T., Woodbury, M. E., Srivastava, G., Möller, T., Hudry, E., Das, S., Saido, T., Karran, E., Hyman, B., Perry, V. H., Fiers, M., & De Strooper, B. (2019). The major risk factors for Alzheimer's disease: Age, sex, and genes modulate the microglia response to A β plaques. *Cell Reports*, 27(4), 1293–1306.e6. <https://doi.org/10.1016/j.celrep.2019.03.099>
- Sherrington, R., Froelich, S., Sorbi, S., Campion, D., Chi, H., Rogaeva, E. A., Levesque, G., Rogaev, E. I., Lin, C., Liang, Y., Ikeda, M., Mar, L., Brice, A., Agid, Y., Percy, M. E., Clerget-Darpoux, F., Piacentini, S., Marcon, G., Nacmias, B., ... St George-Hyslop, P. H. (1996). Alzheimer's disease associated with mutations in presenilin 2 is rare and variably penetrant. *Human Molecular Genetics*, 5(7), 985–988. <https://doi.org/10.1093/hmg/5.7.985>
- Silvin, A., Uderhardt, S., Piot, C., Da Mesquita, S., Yang, K., Geirsdottir, L., Mulder, K., Eyal, D., Liu, Z., Bridlance, C., Thion, M. S., Zhang, X. M., Kong, W. T., Deloger, M., Fontes, V., Weiner, A., Ee, R., Dress, R., Hang, J. W., ... Ginhoux, F. (2022). Dual ontogeny of disease-associated microglia and disease inflammatory macrophages in aging and neurodegeneration. *Immunity*, 55(8), 1448–1465.e6. <https://doi.org/10.1016/j.immuni.2022.07.004>
- Smith, T., Heger, A., & Sudbery, I. (2017). UMI-tools: Modeling sequencing errors in unique molecular identifiers to improve quantification accuracy. *Genome Research*, 27(3), 491–499. <https://doi.org/10.1101/gr.209601.116>
- Takahashi, H., Klein, Z. A., Bhagat, S. M., Kaufman, A. C., Kostylev, M. A., Ikezu, T., & Strittmatter, S. M. (2017). Opposing effects of progranulin deficiency on amyloid and tau pathologies via microglial TYROBP network. *Acta Neuropathologica*, 133(5), 785–807. <https://doi.org/10.1007/s00401-017-1668-z>

- Talma, N., Gerrits, E., Wang, B., Eggen, B. J. L., & Demaria, M. (2021). Identification of distinct and age-dependent p16 high microglia subtypes. *Aging Cell*, 20(10), e13450. <https://doi.org/10.1111/accel.13450>
- Tamura, T., Nagamura-Inoue, T., Shmeltzer, Z., Kuwata, T., & Ozato, K. (2000). ICSBP directs bipotential myeloid progenitor cells to differentiate into mature macrophages. *Immunity*, 13(2), 155–165. [https://doi.org/10.1016/S1074-7613\(00\)00016-9](https://doi.org/10.1016/S1074-7613(00)00016-9)
- Tanaka, Y., Matsuwaki, T., Yamanouchi, K., & Nishihara, M. (2013). Increased lysosomal biogenesis in activated microglia and exacerbated neuronal damage after traumatic brain injury in progranulin-deficient mice. *Neuroscience*, 250, 8–19. <https://doi.org/10.1016/j.neuroscience.2013.06.049>
- Tarkowski, E., Liljeroth, A.-M., Minthon, L., Tarkowski, A., Wallin, A., & Blennow, K. (2003). Cerebral pattern of pro- and anti-inflammatory cytokines in dementias. *Brain Research Bulletin*, 61(3), 255–260. [https://doi.org/10.1016/S0361-9230\(03\)00088-1](https://doi.org/10.1016/S0361-9230(03)00088-1)
- van Weering, H. R. J., Nijboer, T. W., Brummer, M. L., Boddeke, E. W. G. M., & Eggen, B. J. L. (2023). Microglia morphotyping in the adult mouse CNS using hierarchical clustering on principal components reveals regional heterogeneity but no sexual dimorphism. *Glia*, 71, 2356–2371. <https://doi.org/10.1002/glia.24427>
- Vegh, M. J., Heldring, C. M. C. M., Kamphuis, W., Hijazi, S., Timmerman, A. J., Li, K. W., van Nierop, P., Mansvelter, H. D., Hol, E. M., Smit, A. B., van Kesteren, R. E., Végh, M. J., Heldring, C. M. C. M., Kamphuis, W., Hijazi, S., Timmerman, A. J., Li, K. W., van Nierop, P., Mansvelter, H. D., ... van Kesteren, R. E. (2014). Reducing hippocampal extracellular matrix reverses early memory deficits in a mouse model of Alzheimer's disease. *Acta Neuropathologica Communications*, 2(1), 1–11. <https://doi.org/10.1186/s40478-014-0076-z>
- Wightman, D. P., Jansen, I. E., Savage, J. E., Shadrin, A. A., Bahrami, S., Holland, D., Rongve, A., Børte, S., Winsvold, B. S., Drange, O. K., Martinsen, A. E., Skogholt, A. H., Willer, C., Bråthen, G., Bosnes, I., Nielsen, J. B., Fritsche, L. G., Thomas, L. F., Pedersen, L. M., ... Posthuma, D. (2021). A genome-wide association study with 1,126,563 individuals identifies new risk loci for Alzheimer's disease. *Nature Genetics*, 53(9), 1276–1282. <https://doi.org/10.1038/s41588-021-00921-z>
- Wu, T., Hu, E., Xu, S., Chen, M., Guo, P., Dai, Z., Feng, T., Zhou, L., Tang, W., Zhan, L., Fu, X., Liu, S., Bo, X., & Yu, G. (2021). clusterProfiler 4.0: A universal enrichment tool for interpreting omics data. *Innovations*, 2(3), 100141. <https://doi.org/10.1016/j.xinn.2021.100141>
- Yin, F., Banerjee, R., Thomas, B., Zhou, P., Qian, L., Jia, T., Ma, X., Ma, Y., Iadecola, C., Beal, M. F., Nathan, C., & Ding, A. (2010). Exaggerated inflammation, impaired host defense, and neuropathology in progranulin-deficient mice. *Journal of Experimental Medicine*, 207(1), 117–128. <https://doi.org/10.1084/jem.20091568>
- Yin, Z., Raj, D., Saiepour, N., Van Dam, D., Brouwer, N., Holtman, I. R., Eggen, B. J. L., Möller, T., Tamm, J. A., Abdourahman, A., Hol, E. M., Kamphuis, W., Bayer, T. A., De Deyn, P. P., & Boddeke, E. (2017). Immune hyperreactivity of A β plaque-associated microglia in Alzheimer's disease. *Neurobiology of Aging*, 55, 115–122. <https://doi.org/10.1016/j.neurobiolaging.2017.03.021>
- Zeng, Q., Man, R., Luo, Y., Zeng, L., Zhong, Y., Lu, B., & Wang, X. (2017). IRF-8 is involved in amyloid- β 1–40 (A β 1–40)-induced microglial activation: A new implication in Alzheimer's disease. *Journal of Molecular Neuroscience*, 63(2), 159–164. <https://doi.org/10.1007/s12031-017-0966-1>
- Zhang, X., Heng, Y., Kooistra, S. M., Weering, H. R. J., Brummer, M. L., Gerrits, E., Wesseling, E. M., Brouwer, N., Nijboer, T. W., Dubbelaar, M. L., Boddeke, E. W. G. M., & Eggen, B. J. L. (2021). Intrinsic DNA damage repair deficiency results in progressive microglia loss and replacement. *Glia*, 69(3), 729–745. <https://doi.org/10.1002/glia.23925>
- Zhou, N., Liu, K., Sun, Y., Cao, Y., & Yang, J. (2019). Transcriptional mechanism of IRF8 and PU.1 governs microglial activation in

neurodegenerative condition. *Protein & Cell*, 10(2), 87–103. <https://doi.org/10.1007/s13238-018-0599-3>

SUPPORTING INFORMATION

Additional supporting information can be found online in the Supporting Information section at the end of this article.

Figure S1. Morphometric analysis of microglia in CA in 4- and 6-month-old APP/PS1 mice (a) A histogram depicting the number of plaques with different size of A β plaques (μm^2) ($n=3$ mice, 4-month-old APP/PS1 mice: 1 plaque, 6-month-old APP/PS1: 28 plaques in total). (b) A schematic overview of the morphometric analysis performed based on 23 morphological parameters. (c) A heatmap with hierarchical clustering representing the z-score for all morphometric features for each cluster detected. (d) PCA of all selected individual cells with corresponding colors of each cluster. (e) Sholl analysis of microglia from each cluster. (f) The silhouette of one IBA1-labeled microglia in each cluster visualized as a representative image. (g) Bar plot showing frequency of cells per cluster in each condition.

Figure S2. FACS strategy to isolate microglia for bulk RNA-seq Representative FACS plots for the isolation of microglia (PI^{neg}DRAQ5^{pos}CD11b^{high}CD45^{int}CD49d^{neg} cells).

Figure S3. FACS strategy to isolate microglia for scRNA-seq Representative FACS plots for the isolation of CD11c^{neg} and CD11c^{pos} microglia (DAPI^{neg} DRAQ5^{pos} CD11b^{high} CD45^{int} CD11c^{neg/pos}).

Figure S4. scRNA-seq of CD11c^{pos} and CD11c^{neg} microglia in 6-month-old APP/PS1 and WT mice (a) Volcano plots depicting enriched genes in the cluster compared to all other clusters (LFC >.25, adjusted p -value <.05). (b) A bar plot depicting the proportions of the CORTEX cluster in each condition. (c) A bar plot depicting the result of gene ontology analysis (TOP10 enriched Biological Process) of the enriched genes in the CORTEX cluster compared to all other clusters (LFC >.25, adjusted p -value <.05). (d) A sunburst plot depicting significantly enriched synaptic ontology terms (Cellular Component) in SynGO. (e) Violin plots depicting the RNA expression level (Log₂ RNA count) of Clec7a and Cst7 genes. Colors indicate the clusters.

Table S1. A list of the morphometric parameters with explanations.

Table S2. Statistical information.

Table S3. A list of cluster marker genes (related to Figure 3).

Table S4. Synaptic GO analysis of genes enriched in the CORTEX cluster by SynGO (related to Figure S3).

Table S5. A list of the genes in subset 1 and 2 (related to Figure 4).

Data S1. Transparent Science Questionnaire for Authors

How to cite this article: Oshima, T., Kater, M. S. J., Huffels, C. F. M., Wesseling, E. M., Middeldorp, J., Hol, E. M., Verheijen, M. H. G., Smit, A. B., Boddeke, E. W. G. M., & Eggen, B. J. L. (2024). Early amyloid-induced changes in microglia gene expression in male APP/PS1 mice. *Journal of Neuroscience Research*, 102, e25295. <https://doi.org/10.1002/jnr.25295>